Energy Conversion and Management 238 (2021) 114172

Contents lists available at ScienceDirect

Energy Conversion and Management

journal homepage: www.elsevier.com/locate/enconman

Novel hybrid aircraft propulsion systems using hydrogen, methane, methanol, ethanol and dimethyl ether as alternative fuels

Shaimaa Seyam *, Ibrahim Dincer, Martin Agelin-Chaab

Department of Mechenical and Manufacturing Engineering, Ontario Tech University, Oshawa, Ontario L1H 7K4, Canada

ARTICLE INFO

Keywords:
Aircraft
Aviation
Fuels
Energy
Exergy
Solid oxide fuel cell
Turbofan

ABSTRACT

This paper presents a unique hybrid type aircraft propulsion system which combines a commercial turbofan system with a solid oxide fuel cell system. Thermodynamic analyses and parametric studies are collectively performed to investigate the compatibility and applicability of the proposed system as well as its performance through the energetic and exergetic efficiencies to determine how the efficiencies are affected by varying the operating conditions. Hydrogen, methane, methanol, ethanol, and dimethyl ether with different combinations are chosen as alternative fuels to replace kerosene, which is a traditional, fossil-based fuel. It is found that the net power of the solid oxide fuel cell is 944 kW with an electric efficiency of 87.0%. A maximum thermal efficiency of 32.3% and exergetic efficiency of 43.9% were achieved using 75% methane and 25% hydrogen fuel. The maximum overall thermal and exergetic efficiencies of the hybrid turbofan are 48.1% and 54.4%, respectively, using 75% methanol and 25% hydrogen fuel, which reduce carbon emissions by 65% compared to the fossil fuels. Therefore, the hybrid turbofan aircraft engine can increase the turbofan performance. In addition, a fuel mixture of 60% ethanol and 40% hydrogen can increase the performance by 5% and reduce carbon emissions by 73%.

1. Introduction

Aviation is essential for global mobility and plays a vital role in economic activities. The number of passenger and freight flights have significantly increased over the past years due to globalization. The energy use for aviation transportation in Canada, for instance, has increased from 180 to 300 PJ between 1990 and 2019 [1]. This energy use relies on aviation turbo fuels, which are kerosene-based fuels. Consequently, the greenhouse gas (GHG) emissions have increased substantially from 15 to 22 Mt of CO_2e [2,3], which contributes about 2% of total GHG emissions from all transportation sectors in Canada.

Several studies have been conducted on clean aviation transportation. For example, Kousoulidou and Lonza [4] collected data from actual flight information, EUROCONTROL and Eurostat statistics for European flights to predict the consumption of biokerosene and conventional kerosene and their impact on carbon emission. They discovered that the total fuel consumption was about 170 million tonnes resulting in 400 million tonnes of GHG emissions by 2030, and the main contribution to these data is the conventional fuels. Therefore, the European Union planned for the use of biofuels such as clustered in hydroprocessed esters and fatty acids (HEFA), hydrotreated vegetable oils (HVO), and biomass-to-liquid (BTL) biojet fuels in order to reduce the global CO_2 emissions from the aviation sector. Furthermore, Badami et al. [5] conducted experimental and numerical studies on a small-size turbojet engine with a nominal thrust of 80 N. They compared the turbojet performance using a traditional Jet-A with two alternative fuels, such as synthetic gas to liquid and a blended biofuel of Jet-A and Jatropha Methyl Ester. A similar performance was achieved despite the lower heat value for alternative fuels. Aydin et al. [6] investigated the exergetic performance of a TRS18 turbojet drone engine operating using kerosene. They found that the exergetic efficiency was 42%, and the maximum exergy destruction rate occurred for the burner. Other control methods can be used to improve aircraft performance. For example, Yazar et al. [7] used neuro-fuzzy interference system to estimate exhaust gaseous emissions for military aircraft. The system depends on air-fuel ratio, combustion efficiency, and engine speed. It was able to reduce carbon emission without sacrificing the overall engine performance. Also, Hashemi et al. [8] presented an adaptative battery model of lithium-ion-battery for electric or hybrid aircrafts. The model was machine-learning-based model. They discovered that the model achieved accurate fault diagnosis and fault detection applications to improve battery accuracy.

Alternative fuels such as hydrogen and methane have been

* Corresponding author.
E-mail addresses: shaimaa.seyam@ontariotechu.net (S. Seyam), Ibrahim.dincer@uoit.ca (I. Dincer), Martin.Agelin-Chaab@uoit.ca (M. Agelin-Chaab).

https://doi.org/10.1016/j.enconman.2021.114172
Received 25 February 2021; Accepted 14 April 2021
Available online 28 April 2021

Nomenclature

Symbols

A	Area [m^2]
F/A	Fuel-to-air mass ratio [kg_f/kg_a]
h	Specific enthalpy [kJ/kg]
M	Mach number
N	Number of cells
P	Pressure [kPa]
$\dot{Q}$	Heat rate [kW]
s	Specific entropy [kJ/kgK]
T	Temperature [K]
U	Air speed [m/s]
VOC	Voltage-operating current [VA]
$\dot{W}$	Power [kW]

Greek letters

η	Thermal efficiency
ψ	Exergy efficiency
Γ	Thrust force [N]

Abbreviations

SOFC	Solid oxide fuel cell
GT	Gas turbine
SR	Steam reforming
TIT	Turbine inlet temperature
TSEC	Thrust specific fuel consumption
WGS	Water gas shift

Subscript

a	Ambient
e	Exit flow/ electric
eng	Overall engine
i	Inlet flow
in	Inlet heat or work
j	Current density
loss	loss
out	Outlet heat or work

investigated in research to test the ability of operation in aircraft engines. Hydrogen is a carbon-free fuel with a high heating value and high energy carrier with less volume, and methane has a low carbon intensity rating, which can significantly reduce carbon emissions [9]. Adding hydrogen to methane or other hydrocarbon fuels has been tested experimentally. Hydrogen can decrease the ignition delay and increase laminar burning velocities [10]. Some mixtures of ammonia, methane, and hydrogen have been conducted experimentally in a high-pressure combustion test rig for gas turbines. The mixture can achieve high stability flame with low emissions at a low equivalence ratio [11].

Hydrogenation of jet fuels has been studied and tested. Jia et al. [12] investigated the effect of hydrogenation degree on jet fuel (RP-3). Combining hydrogen and additive catalyst has slightly reduced the density and sulfur content but enhanced thermal oxidation stability of jet fuel. In addition, a mixture of hydrogen ammonia and air has been combusted and numerically investigated. Cai and Zhao found that increasing the hydrogen to ammonia ratio to about 50% dramatically decreased the NO_x emission and increased the flame length closer to combustor inlet [13]. Luo et al. [14] studied the addition of hydrogen and fuel additive effects on kerosene for dual-mode scramjet under flight Mach 3.8 inflow conditions. The results showed that adding hydrogen increased the heat released from the scramjet at low combustion conditions yielding to improved combustion efficiency and flame stabilization. Bicer and Dincer [15] performed a life cycle assessment of a well-to-wake approach for conventional and alternative aircraft fuels, such as hydrogen, ammonia, methanol, ethanol, and liquified natural gas. They showed that hydrogen and liquified natural gas have the lowest environmental impact compared to other fuels because of their potential for clean and renewable production.

Fuel cells are introduced into aircraft engines as powering systems to increase engine performance. Few studies have combined solid oxide fuel cell (SOFC) with an aircraft engine. For example, Ji et al. [16] compared thermodynamically three configurations of turbojet engines using kerosene fuel. The configurations are two-shaft turbojet, two-shaft turbojet with afterburner, two-shaft turbojet with SOFC and afterburner. The last design has achieved the best thermal efficiency between 36% and 42% according to different turbine inlet temperatures from 1550 to 1700 K and a pressure ratio of 24. Besides, Waters and Cadou [17] presented three aircraft engines of the unmanned aerial vehicle combined with SOFC and catalytic partial oxidation reactors to reduce the fuel burn. The engines are turbojet, high bypass ratio and low bypass ratio of turbofans. The fuel used in the system is the JP-5. They found that fuel efficiency increased by about 8% for 90 kW high bypass turbofan with a modest cost.

Moreover, Ji et al. [18] conducted their study on unmanned aerial vehicles. They proposed the concept of turbine-less jet engines combined with SOFC and battery to operate the fuel cell. The proposed design showed better performance than a traditional turbojet engine with a maximum pressure ratio of 33 and a Mach number of 0.3. Also, Bakalis et al. [19] studied a hybrid SOFC and gas turbine and conducted an optimization to achieve the best performance in the whole operating range. The optimized hybrid system can produce a net power of 246.4 kW (192.2 kW for SOFC and 57.2 kW for GT) with 58.5% thermal efficiency.

Aircraft manufacturers are concerned about the extra weight that affect the aerodynamic performance of airplanes due to changing fuel types and engine systems. However, studies have proven the opposite. The hybridization of alternating powering systems has been investigated with the associated flight performance as reported in Ji et al. [20]. It is found that the thrust force increasing due to the decrease in fuel consumption the fuel cell during the cruising situation, but the exhaust speed significantly depends the inlet air mass flowrate more than the fuel cell characterizations. Also, Verstraete [21] investigated the utilization of hydrogen fuel in the aviation sector. It was found that hydrogen storage capacity can be performed in a smaller span and wing area. The gross weight of the hydrogen-fueled aircraft can be reduced by 30% compared to kerosene-based fuels, which reduces the direct operating costs from 6.65 to 6.53 ¢/seat. In addition, they confirmed that the improvements in engine-specific fuel consumption were about 20% less sensitive for a hydrogen-fueled than that of kerosene-fueled aircraft. Also, the ratio of operating empty weight between the hydrogen-fuel to kerosene-fuel is 95.9%. Further, the left/drag ratio of the airplane is less by 15.3% for using hydrogen fuel. However, the energy utilization was higher for the hydrogen fuel of 643.4 kJ/seat than that of kerosene fuel by 68%.

The hybrid aircraft engines have been studied in the last decade and still more research is needed to include other fuel cells and different aircraft engines. The novelty of this paper is developing a hybrid turbofan aircraft engine and investigating its performance thermodynamically since turbofan engines are widely used engines in civil aviation in Canadian air transportation. In addition, the government of Canada has a stated goal to strictly reduce emissions from all transportation sectors, including aviation, by 2030 [22]. To contribute to this goal, this paper presents a proposed turbofan engine using the SOFC and compared its performance with that of a traditional turbofan engine. Additionally, the paper conducts thermodynamic analyses using five

alternative fuels, including methane, methanol, ethanol, dimethyl ether, and hydrogen. More specifically, energy and exergy analyses will be performed using alternative fuels.

2. System description

The baseline system is a turbofan aircraft, as shown in Fig. 1, which comprises three spools; the 1-stage fan with a 6-stage low-pressure (LP) turbine (LPT), the 8-stage intermediate-pressure (IP) compressor (IPC) with 1-stage IP turbine (IPT), and the 6-stage high-pressure (HP) compressor (HPC) with a 1-stage HP turbine. The temperature and specific entropy (T-s) diagram is displayed in Fig. 2. The air enters the inlet diffuser, then is first compressed through the fan. After that, some air is bypassed to the fan nozzle to the atmosphere, while another part of air is compressed through the IP- then HP- compressors. A small portion of air is bled for other uses inside the airplane. A fuel mixture is combusted with air at high pressure and temperature, then the exhaust gas is expanded through the HP-, IP-, and LP-turbines. The exhaust gas exits the exit nozzle to produce the thrust force. The fuel used in the aviation system is kerosene with a chemical formula of $C_{10}H_{22}$. The power generated from the gas turbine (GT) system is used to operate the cockpit of the airplane, and auxiliary systems, and battery for storage and emergency cases. A turbofan aircraft engine is running the Boeing 787 Dreamline in Air Canada. The specifications of the turbofan are listed in Table 1.

The hybrid solid oxide fuel cell (SOFC) and turbofan consist of a turbofan aircraft engine with a high bypass ratio (high-BPR) and a SOFC, as shown in Fig. 3. The airflow enters the diffuser and some of the air is bypassed around the GT tell the high-pressure compressors to the atmosphere, while the remaining air flows through the GT. The compressed air from the IPC and HPC compressors flows through the cathode of the SOFC and the combustion chambers. The fuel blend and the steam enter the reformer and the anode of the SOFC. The exit flows from the SOFC burn with the compressed air in the combustion chamber. The exhaust gases are flow through the HPT turbine, then the LPT turbine, and the hot exit nozzle.

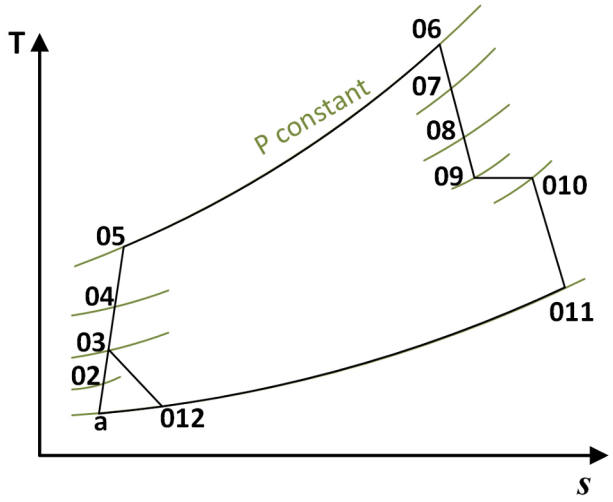

Fig. 2. T-s diagram for a base-turbofan engine.

3. Methods

The thermodynamic analysis is conducted to investigate the performance of the hybrid turbofan engines. The following subsections explain the modeling of the turbofan engine, SOFC, and fuel combustion.

3.1. Modeling of the turbofan engine

The ambient condition varies according to the altitude (Z), and both of them decrease with increasing the altitude. The ambient temperature T_a and ambient pressure P_a are described below:

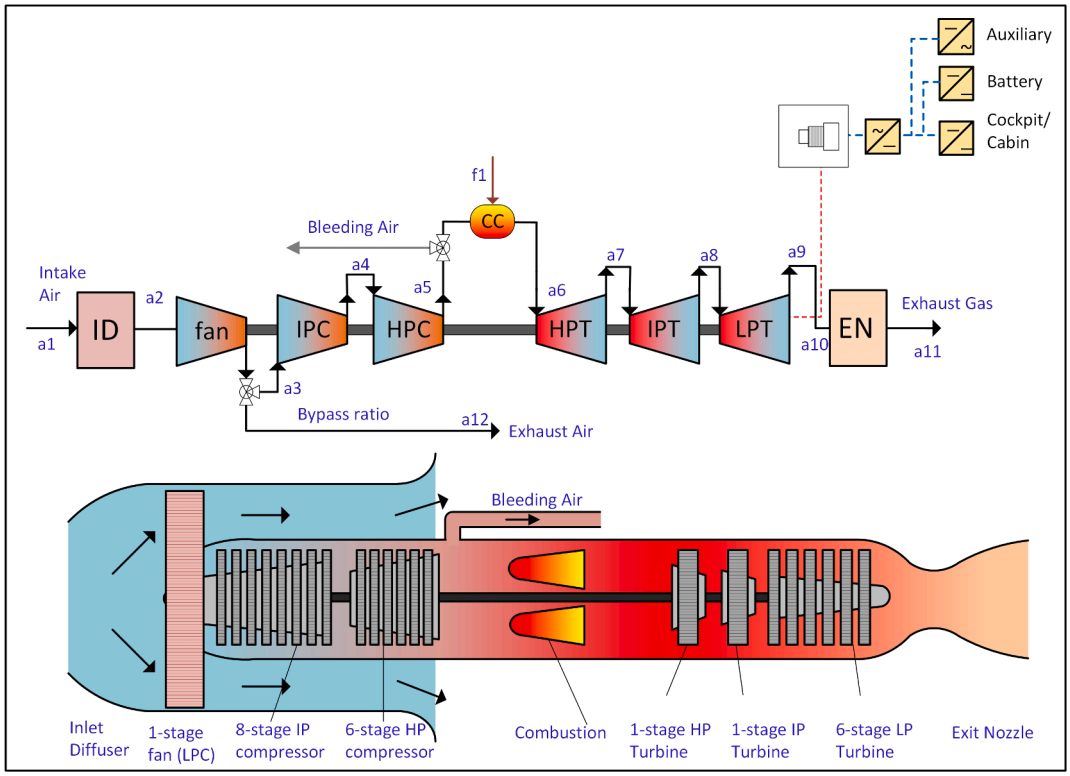

Fig. 1. Configuration of the base turbofan.

Table 1
Specification of turbojet and turbofan aircraft engines.

Specifications	Turbofan [23]		
Aircraft engine	Rolls-Royce Trent 1000		
General Characteristics			
Type	Three-spool high-bypass turbofan		
Dimension	Length: 4.738 m, diameter: 2.85 m (fan)		
Dry weight	5,936 – 6,120 kg		
Components			
Compressor	One-stage LP (fan), 8-stage IP, 6-stage HP compressor		
Combustors	Single annular combustor with 18-off fuel spray nozzles		
Turbine	Single-stage HP (13391 RPM), single-stage IP turbine (8937 rpm), and 6-stage LP turbine (2683 rpm)		
Air bleeding	2% after the HP compressor and before the combustors.		
Performance			
Overall pressure ratio	50:1	SFC take-off	479.16 kg/(h.kN)
TIT	1800 K	Air mass flow	1,090 – 1,210 kg/s
Thrust take-off	265.3–360.4 kN	BPR	greater than10:1

TIT: Turbine inlet temperature, SFC: Specific fuel consumption, BPR: Bypass ratio

$$T_a = 288.15 + L_a Z \;\&\; P_a = 101.325\left(\frac{288.15}{T_a}\right)^{\frac{g}{R_a L_a}} \tag{1}$$

where L_a is the base temperature lapse rate per kilometer of geopotential altitude and equals to −6.5 K/km, g is the gravitational acceleration, R_a is the gas constant of air in J/kg.K. The flight speed is defined as $U_a = M\sqrt{\gamma R_a T_a}$, where M is a Mach number, γ is the specific heat ratio of air (1.4). The inlet air temperature to the diffuser is described as in Eq. (2):

$$T_{02} = T_a\left(1 + \frac{\gamma-1}{2}M^2\right), \quad P_{02} = P_a\left(1 + \frac{\gamma-1}{2}M^2\right)^{\frac{\gamma}{\gamma-1}} \tag{2}$$

The energy balance and exergy balance equations for the components in the turbofan engine are shown in Table 2. The isentropic efficiencies are 90% for turbines and compressors and 87% for hot and fan nozzles. The percentage total pressure drops in the combustion chamber relative to the HPC is 2%, and the percentage pressure losses in the jet pipe relative to the LPT is 20%.

The hot nozzle and fan nozzle should be checked for chocking pressure, P_C, which is estimated from the following equation:

$$\frac{P_i}{P_C} = \frac{1}{\left[1 - \left(\frac{1}{\eta_n}\right)\left(\frac{\gamma-1}{\gamma+1}\right)\right]^{\frac{\gamma}{\gamma-1}}} \tag{3}$$

where η_n is the nozzle efficiency. If the ratio of nozzle inlet pressure P_i to the ambient pressure $P_a$is greater than P_i/P_C, then the nozzle is choking. Therefore, the nozzle exit pressure P_e, temperature T_e, and speed U_e are calculated from the following equations:

$$P_e = \frac{P_i}{P_i/P_C}, \quad T_e = T_i\frac{2}{\gamma+1}, \quad U_e = \sqrt{\gamma R_a T_e} \tag{4}$$

The general form of the second law of thermodynamics can be

Table 2
Energy and exergy balance equations for basic components in turbofan engines.

Components	Energy balance	Exergy balance
Inlet Diffuser	$\dot{m}_{i,d}\left(h_{i,d}+\frac{U_a^2}{2}\right) = \dot{m}_{e,d}\left(h_{e,d}+\frac{U_{02}^2}{2}\right)$	$\dot{m}_{i,d}ex_{i,d} + \dot{m}_{i,d}\frac{U_a^2}{2} = \dot{m}_{e,d}ex_{e,d} + \dot{m}_{e,d}\frac{U_{02}^2}{2} + \dot{E}x_{D,d}$
Compressors	$\dot{W}_c = \dot{m}_c(h_{e,c} - h_{i,c})/\eta_c$	$\dot{m}_{i,c}ex_{i,c} + \dot{W}_c = \dot{m}_{e,c}ex_{e,c} + \dot{E}x_{D,c}$
Turbines	$\dot{W}_t = \eta_t\dot{m}_t(h_{i,t} - h_{e,t})$	$\dot{m}_{i,t}ex_{i,t} = \dot{W}_t + \dot{m}_{e,t}ex_{e,t} + \dot{E}x_{D,t}$
Exit Nozzle	$\dot{m}_{i,n}\left(h_{i,n}+\frac{U_s^2}{2}\right) = \dot{m}_{e,n}\left(h_{e,n}+\frac{U_n^2}{2}\right)$	$\dot{m}_{i,n}ex_{i,n} + \dot{m}_{i,n}\frac{U_s^2}{2} = \dot{m}_{e,n}ex_{e,n} + \dot{m}_{e,n}\frac{U_n^2}{2} + \dot{E}x_{D,n}$
Reactors	$\sum_R\dot{m}_{in,R}h_{in,R} + \dot{Q}_{i,r} = \sum_P\dot{m}_{e,P}h_{e,P}$	$\sum_R\dot{m}_{i,R}ex_{i,R} + (T_o/T_s - 1)\dot{Q}_{i,r} = \sum_P\dot{m}_{e,P}ex_{e,P} + \dot{E}x_{D,r}$

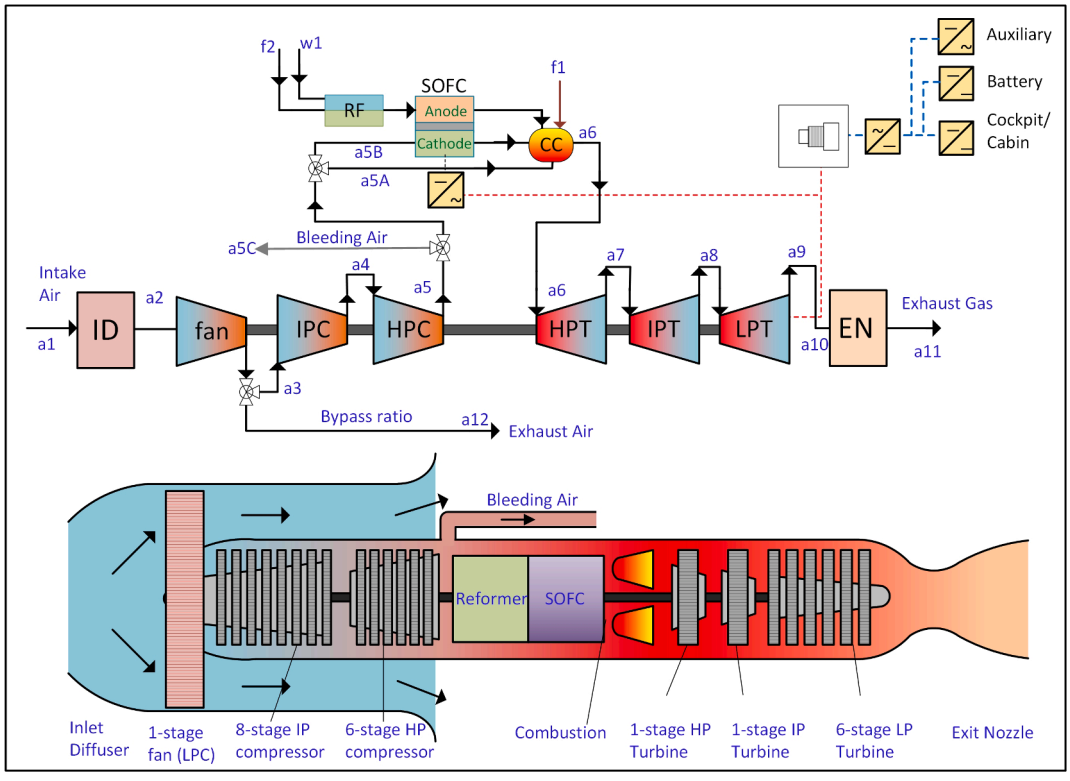

Fig. 3. Hybrid SOFC-turbofan engine.

represented by the exergy balance equations in a steady-state condition for each process. It can be written as follows:

$$\sum_i \dot{m}_i ex_i + \sum_{in} \dot{E}x_Q + \sum_{in} \dot{E}x_W + \sum_{in} \dot{E}x_{KE} = \sum \dot{m}_e ex_e + \sum_{out} \dot{E}x_Q + \sum_{out} \dot{E}x_W + \sum_{out} \dot{E}x_{KE} + \dot{E}x_D \quad (5)$$

where $\dot{m}_i$ and $\dot{m}_e$ are the inlet and exit mass flow rates to and from a system, $\dot{E}x_D$ refers to the exergy destruction rate, $\dot{E}x_W$ denotes the work done or required by the process, $\dot{E}x_{KE}$ is the kinetic exergy and $\dot{E}x_Q$ is thermal exergy due to the heat transfer within the boundaries ($\dot{Q}_{cv,i}$) and depends on the reference temperature T_o. Also, $T_{s,i}$ is the source temperature, and U is the air speed. These can be defined as follows:

$$\dot{E}x_{KE} = \frac{\dot{m}U^2}{2},\ \dot{E}x_W = \dot{W}_{cv},\ \dot{E}x_{Q,i} = \left(1 - \frac{T_o}{T_{s,i}}\right)\dot{Q}_{cv,i} \quad (6)$$

The molar specific exergy of each stream is comprised of molar specific physical exergy, $\overline{ex}_{ph,i}$, and molar specific chemical exergy, $\overline{ex}_{ch,i}$, and are described as follows:

$$\overline{ex}_i = \overline{ex}_{ph,i} + \overline{ex}_{ch,i} = \sum_i \left[\left(\overline{h}_i - \overline{h}_o\right) - T_o\left(\overline{s}_i - \overline{s}_o\right)\right] + \sum_i n_i\left(\overline{g}_f^o + \overline{g}_{T_o} - \overline{g}^o\right) \quad (7)$$

Note that the physical specific exergy depends on the specific enthalpy and entropy for a substance at a specific temperature and pressure, while the chemical exergy depends on the chemical changes of a component composition during the chemical reactions. It depends on the Gibbs function of a unit mole of a substance $\overline{g}$, which consists of the Gibbs function of formation of each substance $\overline{g}_f^o$, Gibbs function of a substance at a specific temperature $\overline{g}_{T_o}$, and Gibbs function at a reference temperature $\overline{g}^o$.

The net power of the gas turbine can be determined as the difference between the total power of turbines and the total required power of compressors, which is defined below:

$$\dot{W}_{GT} = \sum \dot{W}_T - \sum \dot{W}_C \quad (8)$$

The thrust force of the turbofan, Γ, is defined as in Eq. (9) in the general form. The total thrust force is the summation of the fan thrust force from the exit fan nozzle at state point 11 and the hot thrust force from the exit nozzle at state point 12.

$$\Gamma = \sum_k \dot{m}_{e,k} U_{e,k} - \sum_k \dot{m}_{e,k} U_{e,k} - \sum_k A_{e,k}\left(P_{e,k} - P_a\right) \quad (9)$$

The thrust specific fuel consumption (TSFC) is defined by the ratio of fuel mass flow rate to the thrust force and determined as:

$$\mathrm{TSFC} = \frac{\dot{m}_f}{\Gamma} \quad (10)$$

The energetic and exergetic efficiencies of turbofan are described as

$$\eta_{GT} = \frac{\dot{W}_{GT} + \Gamma U_a}{\dot{Q}_{CC}} \ \&\ \psi_{GT} = \frac{\dot{W}_{GT} + \Gamma U_a}{\dot{E}x_{CC}^Q} \quad (11)$$

The aviation base fuel is kerosene-based fuel, which can be expressed as kerosene with a chemical formula of $C_{10}H_{22}$.

3.2. Modeling of the solid oxide fuel cell

The fuel mixture is mixed with steam and flows to the SOFC anode. The air is flowing to the SOFC cathode. The oxygen molecules diffuse to the triple-phase boundary to receive the electrons and produce oxygen ions O^{2-}, which are move to the anode to produce electric current. The oxygen is released from the cathode to exit the fuel cell. The oxygen ions react with hydrogen to produce water on the anode side. The specifications of SOFC is listed in Table 3. The electrochemical reactions of the SOFC are listed below:

- Anode: $H_2 + O^{2-} \rightarrow H_2O + 2e^-$
- Cathode: $0.5\ O_2 + 2e^- \leftrightarrow O^{2-}$
- Overall: $H_2 + 0.5\ O_2 \leftrightarrow H_2O$

The cell voltage of the SOFC is expressed as the Nernst potential subtracting the activation losses (η_{act}), the concentration losses (η_{con}), and ohmic losses (η_{ohm}), as shown in Eq. (12).

$$V_{cell} = -\frac{\Delta\overline{g}}{2F} - \frac{\overline{R}T}{2F}\ln\left(\frac{P_{H_2O,an}}{P_{H_2,an}\sqrt{P_{O_2,ca}}}\right) - \eta_{act} - \eta_{con} - \eta_{ohm} \quad (12)$$

where $\Delta\overline{g}$ is the Gibbs free energy [J/mol]; F is the Faraday constant (96,485 C/mol), $\overline{R}$ is the molar gas constant (8.314 J/mol.K), and P is the partial pressure at each electrode in bar.

The activation polarization is produced to overcome the reaction energy barriers between electrode and electrolyte, which are solved using the Butler-Volmer Equation [24,25]. The activation losses occurred on the anode ($\eta_{act,an}$) and cathode ($\eta_{act,ca}$) as shown in Eq. (13), where α_{an} and α_{ca} are the charge transfer coefficients of anode and cathode, respectively.

$$\eta_{act} = \eta_{act,an} + \eta_{act,ca} = \frac{\overline{R}T}{2\alpha_{an}F}\sinh^{-1}\left(\frac{j}{2\ j_{0,an}}\right) + \frac{\overline{R}T}{2\alpha_{ca}F}\sinh^{-1}\left(\frac{j}{2\ j_{0,ca}}\right) \quad (13)$$

Here, j is the current density of the cell. Also, $j_{0,an}$ and $j_{0,ca}$ are the electrode exchange current densities for the anode and cathode, respectively. They are expressed using the Arrhenius' law function of the partial pressure of the reacting species in Eq. (14) and (15) [26]. The γ_{an} and γ_{ca} are the pre-exponential factors, and $E_{act,an}$ and $E_{act,ca}$ are the activation energy for the electrode reactions, and P_{ref} is the reference atmospheric pressure.

$$j_{0,an} = \gamma_{an}\left(\frac{P_{H_2}}{P_{ref}}\right)\left(\frac{P_{H_2O}}{P_{ref}}\right)\exp\left(-\frac{E_{act,an}}{\overline{R}T}\right) \quad (14)$$

$$j_{0,ca} = \gamma_{ca}\left(\frac{P_{O_2}}{P_{ref}}\right)^{0.25}\exp\left(-\frac{E_{act,ca}}{\overline{R}T}\right) \quad (15)$$

The ohmic loss is calculated from Eq. (16) considering four

Table 3
Specifications of the SOFC.

Parameter		SOFC	Units
Operating pressure		200	kPa
Operating temperature		1123	K
Current density, j		350	mA/cm^2
Active cell area, A_{cell}		900	cm^2
N_{cell} in one stack		100 cells	—
Anode thickness, δ_{an}		5.0E-04	m
Cathode thickness, δ_{ca}		5.0E-05	m
Electrolyte thickness, δ_{el}		1.0E-05	m
Interconnect thickness, δ_{in}		1.0E-05	m
Pre-exponential coefficient for anode, γ_{an}		7.0×10^9	A/m^2
Pre-exponential coefficient for cathode, γ_{ca}		2.9×10^9	A/m^2
Anode activation energy, $E_{act,an}$		120,000	J/mol
Cathode activation energy, $E_{act,ca}$		120,000	J/mol
Pore diameter for anode and cathode, r		5.0E-07	m
Porosity of anode, ε_{ca}		0.5	%
Porosity of cathode, ε_{ca}		0.5	%
Tortuosity for anode and cathode, ξ		6	—
Fuller diffusion volume, ν	H_2	7.07	—
	H_2O	12.7	—
	O_2	16.6	—
	N_2	17.9	—

resistances to the flow of ions and electrons inside the anode ($\rho_{an}\delta_{an}$), cathode ($\rho_{ca}\delta_{ca}$), electrolyte ($\rho_{el}\delta_{el}$), and interconnections ($\rho_{in}\delta_{in}$). They are functions of specific material resistivity ρ and the component thickness δ for planar SOFC.

$$\eta_{ohm} = j(\rho_{an}\delta_{an} + \rho_{ca}\delta_{ca} + \rho_{el}\delta_{el} + \rho_{in}\delta_{in}) \tag{16}$$

The concentration losses are the voltage drop caused by the mass transfer of the gas phase into and through the electrode [26]. They are given by the following equations for the anode as Eq. (17) and cathode as Eq. (18):

$$\eta_{con,an} = -\frac{\overline{R}T}{2F}\ln\left(1 - \frac{j}{j_{L,an}}\right) + \frac{\overline{R}T}{2F}\ln\left(1 + \frac{P_{H_2}\, j}{P_{H_2O}\, j_{L,an}}\right) \tag{17}$$

$$\eta_{con,ca} = -\frac{\overline{R}T}{2F}\ln\left(1 - \frac{j}{j_{L,ca}}\right) \tag{18}$$

The limiting current densities are defined for the anode, $j_{L,an}$,and cathode, $j_{L,ca}$, as follows:

$$j_{L,an} = \frac{2FP_{H_2}D_{an(\text{eff})}}{\overline{R}T} \;\; \& \;\; j_{L,ca} = \frac{2FP_{O_2}D_{ca(\text{eff})}}{\overline{R}T} \tag{19}$$

where the $D_{an(\text{eff})}$ and $D_{ca(\text{eff})}$ are the effective diffusivities of reactant species through the porous anode and cathode, respectively. The ordinary diffusion coefficient of each gas, $D_{O,ik}$, is evaluated using Eq. (20) and converted into an effective value, $D_{O,i(\text{eff})}$, using Eq. (21) by considering the porosity (ε) and the tortuosity (ξ) of the electrode pores. Note that M_i and M_k are the corresponding molecular weight of species [kg/kmol] and P is the operating pressure of the fuel cell.

$$D_{O,ik} = \frac{1 \times 10^{-7} T^{1.25}\left(M_i^{-1} + M_k^{-1}\right)^{0.5}}{P\left(\nu_i^{1/3} + \nu_k^{1/3}\right)} \tag{20}$$

$$D_{O,i(\text{eff})} = D_{O,i}\left(\frac{\varepsilon}{\xi}\right) \tag{21}$$

The Fuller volume, ν, is applied to Eq. (20) [27] the i and k refers to the mixture H_2 and H_2O used for the anode and O_2 and N_2 mixture for the cathode. The ν is the Fuller diffusion volume of each gas. The Knudsen diffusion coefficients, $D_{K,i}$, were calculated and converted into effective values as $D_{k,i(\text{eff})}$ in Eq. (23).

$$D_{K,i} = 97\, r\sqrt{\frac{T}{M_i}} \tag{22}$$

$$D_{K,i(\text{eff})} = D_{K,i}\left(\frac{\varepsilon}{\xi}\right) \tag{23}$$

The overall diffusion coefficient, $D_{i(\text{eff})}$, was calculated harmonically averaging the Knudsen effective diffusion coefficient, $D_{K,i(\text{eff})}$, and the ordinary effective diffusion coefficient, $D_{O,i(\text{eff})}$, as described below:

$$\frac{1}{D_{i(\text{eff})}} = \frac{1}{D_{K,i(\text{eff})}} + \frac{1}{D_{O,i(\text{eff})}} \tag{24}$$

Therefore, the effective diffusivities of anode, $D_{an}D_{(\text{eff})}$, and cathode, $D_{ca(\text{eff})}$, are described below:

$$D_{an(\text{eff})} = \left(\frac{P_{H_2O}}{P_{an}}\right)D_{H_2(\text{eff})} + \left(\frac{P_{H_2}}{P_{an}}\right)D_{H_2O(\text{eff})} \;\; \& \;\; D_{ca(\text{eff})} = D_{O_2(\text{eff})} \tag{25}$$

The resultant power output of a fuel cell is presented as follows:

$$\dot{W}_{SOFC,AC} = jA_{\text{cell}}V_{\text{cell}}N_{\text{cell}}\xi_{DC-AC} \tag{26}$$

where A_{cell} is the total active area of a fuel cell in cm^2, N_{cell} is the number of cells, ξ_{DC-AC} is the inverter efficiency from direct current (DC) to alternating current (AC) and is equivalent to 0.95. The electric efficiency of a fuel cell can be determined as Eq. (27), while the thermal energetic and exergetic efficiencies can be evaluated as Eq. (28). The added heat of fuel cell, $\dot{Q}_{SOFC,add}$, is considered as the summation of the added heat through the anode and cathode.

$$\eta_{SOFC,e} = \frac{\dot{W}_{SOFC,AC}}{\dot{W}_{SOFC,AC} + \dot{W}_{SOFC,loss}} \tag{27}$$

$$\eta_{SOFC,th} = \frac{\dot{W}_{SOFC,AC}}{\dot{Q}_{SOFC,add}} \;\; \& \;\; \psi_{SOFC,th} = \frac{\dot{W}_{SOFC,AC}}{\dot{E}x^{Q}_{SOFC,add}} \tag{28}$$

The performance of the developed turbofan systems can be determined as the overall energetic efficiency η_{eng}, and the overall exergetic efficiency ψ_{eng}, as

$$\eta_{eng} = \frac{\dot{W}_{SOFC,AC} + \dot{W}_{GT} + \Gamma U_a}{\dot{Q}_{CC} + \dot{Q}_{SOFC,add} + \dot{Q}_{SR} + \dot{Q}_{WGS}} \tag{29}$$

$$\psi_{eng} = \frac{\dot{W}_{SOFC,AC} + \dot{W}_{GT} + \Gamma U_a}{\dot{E}x^{Q}_{CC} + \dot{E}x^{Q}_{SOFC,add} + \dot{E}x^{Q}_{SR} + \dot{E}x^{Q}_{WSG}} \tag{30}$$

3.3. Combustion modeling

The baseline fuel for the baseline system is kerosene. The alternative fuels selected are hydrogen (H_2), methanol (CH_3OH), and ethanol (CH_3OHCH_2) from monohydric alcohols, dimethyl-ether (DME) (CH_3OCH_3) from ethers, and natural gas which is considered from hydrocarbons and presented as pure methane (CH_4). Their properties are listed in Table 4. They are environmentally benign and have high ignition temperatures [28–31]. The Stoichiometric combustion reactions for the baseline fuel and alternative fuels are listed in Table 5. In this paper, five combinations of fuels are used in the study based on the mass fractions: F1 (75% natural gas and 25% hydrogen); F2 (75% methanol and 25% hydrogen); F3 (60% ethanol and 40% hydrogen); F4 (60% DME and 40% hydrogen); and F5 (15% methane, 40% hydrogen, 15% methanol, 15% ethanol, and 15% DME). The steam reforming (SR) and water gas shift (WGS) for the five combination fuels are listed in Table 6. The combustion reaction in the combustion chamber have excess air of 20% with complete combustion for all alternative fuels and kerosene fuel, which are close to real cases. In addition, the chemical reactions of fuels are based on steady state reactions. Therefore, any interstate reactions are not considered in this paper. In addition, the formation of carbon monoxide in the steam reforming will be converted to carbon dioxide and steam in the water gas shift. Also, the steam reforming and water gas shift utilize 80% of the fuels that means there are some of unburned CO that will be burned in the combustion chamber, which results in lowering the carbon emissions.

The proposed method is thermodynamic analysis of the hybrid turbofan, which is the base analysis of the turbomachinery field. The thermodynamic analysis is very important step because it provides an energetic and exergetic analysis of the proposed system, which analyzes the system performance and capabilities. Other analyses such as exergoeconomic and exergoenvironmental analyses can be applied in near future but out of the current paper scope.

4. Results and discussion

In this section, the thermodynamic analyses and parametric studies are investigated on the base engine and hybrid turbofan. They are discussed below.

4.1. Results of thermodynamic analysis

The base and the SOFC-turbofan engines are modeled using the Aspen Plus, which is illustrated in Fig. 4. The equation of state is chosen

Table 4
Specifications of alternative fuels for the proposed transportation systems.

Specifications	DME [32]	Ethanol [33]	Hydrogen [34]	Methane [35]	Methanol [36]	Kerosene [37]
Molecular formula	CH_3OCH_3	CH_3OHCH_2	H_2	CH_4	CH_3OH	$C_{10}H_{22}$
Molecular weight, M_i [kg/kmol]	46.07	46.07	2.016	16.043	46.069	142
Adiabatic flame temperature [°C]	2100	2082	2000	1963	1949	2093
Auto-ignition temperature [°C]	350	365	571	537	470	640
Density at 40 °C [kg/m^3]	2.11	789	0.0773	0.657	792	760–810
Viscosity at 40 °C [mm^2/s]	0.184	1.056	109	18.72	0.75	1–1.9
High heating value [MJ/kg]	31.67	29.7	141.9	55.5	22.7	46.2
Low heating value [MJ/kg]	28.87	26.7	119.0	50	18.1	43.0

Table 5
Stoichiometric combustion reactions for the fuels.

Fuel	Stoichiometric combustion reaction	$\Delta\bar{h}^0_{298K}$ [kJ/mol]
Kerosene	$C_{12}H_{24} + 18\ O_2 \rightarrow 12\ CO_2 + 12\ H_2O$	−7674.5
Hydrogen	$2\ H_2 + O_2 \rightarrow 2\ H_2O$	−286
Methane	$CH_4 + 2\ O_2 \rightarrow CO_2 + 2\ H_2O$	−891
Methanol	$CH_3OH + 1.5\ O_2 \rightarrow CO_2 + 2\ H_2O$	−726
Ethanol	$CH_3OHCH_2 + 3\ O_2 \rightarrow 2\ CO_2 + 3\ H_2O$	−1366.91
DME	$CH_3OCH_3 + 3\ O_2 \rightarrow 2\ CO_2 + 3\ H_2O$	−2726.3

Table 6
Steam reforming and water gas shift hybrid the SOFC turbofan.

Fuels	SR	WGS
F1	$CH_4 + H_2O \rightarrow CO + 3\ H_2$	$CO + H_2O \rightarrow CO_2 + H_2$
F2	$CH_3OH \rightarrow CO + 2\ H_2$	$CO + H_2O \rightarrow CO_2 + H_2$
F3	$CH_3OHCH_2 \rightarrow CH_4 + CO + H_2$ $CH_4 + H_2O \rightarrow CO + 3\ H_2$	$CO + H_2O \rightarrow CO_2 + H_2$
F4	$CH_3OCH_3 \rightarrow CH_4 + CO + H_2$ $CH_4 + H_2O \rightarrow CO + 3\ H_2$	$CO + H_2O \rightarrow CO_2 + H_2$
F5	$CH_4 + H_2O \rightarrow CO + 3\ H_2$ $CH_3OH \rightarrow CO + 2\ H_2$ $CH_3OHCH_2 \rightarrow CH_4 + CO + H_2$ $CH_3OCH_3 \rightarrow CH_4 + CO + H_2$	$CO + H_2O \rightarrow CO_2 + H_2$

to be Soave-Redlick-Kwong (SRK) for thermodynamic properties because it is the most-widely accepted equation for modern chemical processes and recommended for gas mixture [38–40]. The turbofan is modeled using isentropic compressors and turbines and an expansion valve for modeling the nozzle. Separate stoichiometric reactions are used for SOFC, WGS, and SR. According to the specifications of the turbofan Rolls-Royce Trent 1000, the turbofan has an overall pressure of 50 and a bypass ratio of 10:1. The inlet mass flow rate to the fan is selected to be 1210 kg/s. The airplane is assumed to be in cruising condition at 10 km altitude, at which the ambient conditions are 293.2 K and 26.4 kPa. The Mach number at this altitude for the Boeing 747 Dreamline is 0.83.

The thermodynamic analysis of turbomachinery has been conducted using ideal gas equations as reported [18,41]. The Aspen Plus is a popular software that used in chemical and thermodynamic simulations for power plants and process systems, but it has been rarely used in aviation systems. Therefore, an error analysis has been made between the ideal gas equations (IGE) and Aspen plus simulation (APS) to compare the results, as shown in Table 7, which compares the results of a traditional turbofan using kerosene fuel. The error percentage varies from 0% for combustion chamber to 10.3% for IPC, which are accepted. In addition, the results of Aspen Plus was compared to experimental results of SOFC using methane fuel with error percentage of 2–5% [42]. This variation results from the practical applications of Aspen Plus. In addition, the values of enthalpy and exergy, as shown in Table 8, are calculated based on reference enthalpy and reference exergy, which are the standard conditions of air (298 K and 101.3 kPa) [43]. These reference values are cancelled because the net power of components and the thrust force are calculated based on the difference of inlet and exit conditions. Therefore, the values of enthalpy and exergy are considered to be correct since the error percentage are less than or equal to 10%.

The thermodynamic results are listed for the base-turbofan engine, as shown in Table 8. The inlet air conditions to the inlet diffuser are 253.9 K, 40.7 kPa, and 1210 kg/s resulting in the inlet air speed (U_a) of 248.6 m/s. The air exits from two ports: fan nozzle and hot nozzle. Consequently, the exit air conditions of the fan nozzle at state 12 are 233.2 K, 27.1 kPa, and 1099.9 kg/s, while the exhaust conditions at the hot nozzle at state 11 are 1127.5 K, 83.6 kPa, and 113.9 kg/s. Therefore, the airspeed at the fan nozzle exit (U_{12}) and hot nozzle exit (U_{11}) are 306.1 m/s and 607.8 m/s, respectively. The exergy results are the summation of specific chemical exergy and physical exergy of each component in each state point as explained in Eq. (7), and the Gibbs numbers and the physical exergy are calculated using Aspen Plus. The choking pressure ratio was checked at the exit nozzles to be 2.046 for the hot nozzle and 2.105 for the and fan nozzle. It is found that the inlet to exit pressure ratio is higher for both nozzles, meaning that the thrust force counts for both speed and pressure difference between inlet and exit air.

In addition, the power and heat for components are displayed in Table 9. Since the turbofan is designed to have three spools, each spool carries a compressor and a turbine. Therefore, the turbine should deliver more power than that the corresponding required compressor, so the gas turbine configuration can provide net power to operate other systems in an airplane.

Furthermore, the base-turbofan can deliver a net power of 9144.1 kW and thrust energy of 38182.5 kW, but it requires 109082.6 kW of combustion heat to burn 6 kg/s kerosene fuel. The overall energetic and exergetic efficiencies are 43.4% and 52.0%, respectively.

The solid oxide fuel cell and steam reformer, and water gas shit are added to the turbofan as shown in Fig. 3, which are simulated using the Aspen Plus as in Fig. 4-b. The SR and WGS are operated at 673 and 873 K, respectively. The SR uses the heat of 1789 kW with thermal and exergetic efficiency of 78% and 80%, respectively. Also, the WGS needs a total heat of 112 kW with 65% for both thermal and exergetic efficiencies. The results of the SOFC are presented below in Table 10 for F1, a mixture of 75% methane and 25% hydrogen. The net power of the SOFC is 944 kW with electric efficiency of 87.0%, the thermal efficiency of 32.3%, and exergetic efficiency of 43.9%.

4.2. Discussion of the specific effects on the performance

In this subsection, we discuss some parametric studies that applied on hybrid turbofan engine to understand the performance of turbofan engines. The discussion includes the effect of fuels on the SR, WGS, SOFC, and overall efficiencies, as well as the effect of fuel mass flow rate and combustion pressure, which are discussed below.

4.2.1. Effect of fuels on the performance of steam reforming, water gas shift, and solid oxide fuel cell

Note that five alternative fuels are used in different combinations with hydrogen as in F1 to F5. All the fuels are used under the same turbofan conditions, which are inlet air conditions, inlet conditions and pressure ratio of compressors, combustion pressure and temperature, and the turbine pressure ratios. Regarding the reactors, the temperature

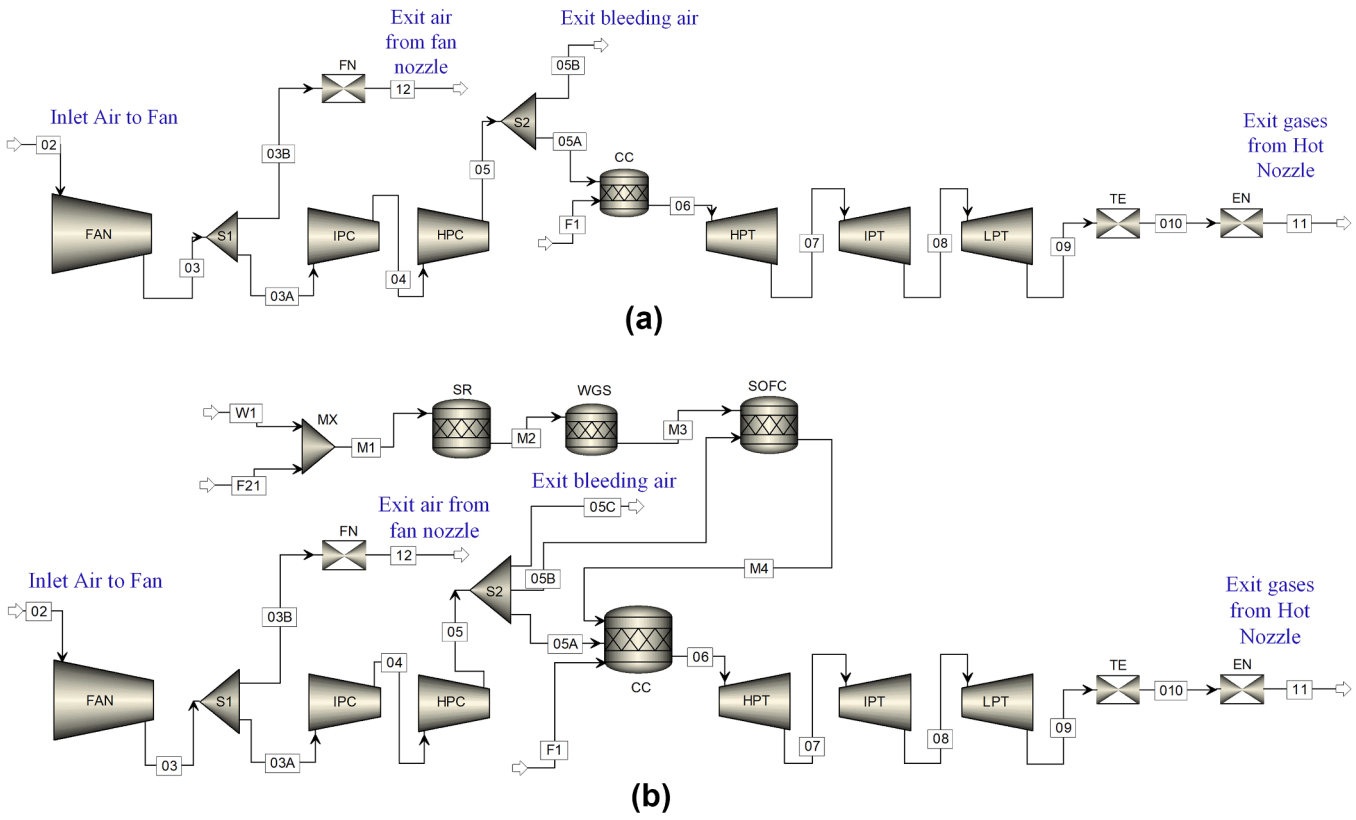

Fig. 4. The Aspen Plus flow chart for the base-turbofan and the SOFC-turbofan systems.

Table 7
Error analysis of traditional turbofan engine between IGC and APS.

Components	IGE	APS	ER [%]
Compressor Power [kW]			
FAN	31180.7	31547.2	1.2
IPC	20844.2	22981.5	10.3
HPC	36066.9	39545.6	9.6
Combustion Heat [kW]			
CC	109082.6	109082.6	0.0
Turbine Power [kW]			
HPT	40755.6	44650.2	9.6
IPT	23970.8	25274.8	5.4
LPT	31180.7	33293.4	6.8
Thrust force [kN]			
EN	89.5	83.7	−6.5
FN	68.94	69.9	1.4

IGE … Ideal gas equations, APS … Aspen Plus simulation, ER … error percentage

of SR and WGS remain constant at 673.2 K and 873.2 K, respectively. The performance of the SR, WGS, and SOFC are affected by the fuel combinations are shown in Table 11. For the SR, the maximum heat is used for F5, which is 1260.9 kW, while the minimum heat is required for F2 to be 1084.2 kW. The best performance of the SR occurs when using methane and hydrogen mixture of F1, achieving about 78% and 80% of thermal and exergetic efficiencies, respectively. The performance of the SR has been decreased from 55% to 45% as F5, F2, F3, and F4 in this order. For the WSG, the required heat varies from 433.8 kW for F2 to 111.8 kW for F1, fulfilling thermal and exergetic efficiencies of about 60% for F5 to 90% for F2. For SOFC, the minimum heat required occurs using F1 to be 2928 kW to achieve a thermal efficiency of 32.3% and exergetic efficiency of 43.9%. However, the maximum heat required can be obtained using F3 to be 3959 kW with thermal and exergetic efficiencies of 23.9% and 32.5%, respectively. Two reasons for this performance variations are: (a) the mass flowrates of fuels entering the SR with respect to the steam mass flow rate (0.2 kg/s), as shown in Table 12, and (b) the chemical reactions of fuel mixture to produce CO and H_2 in the SR which will be reacted to produce CO_2 and H_2 in the WSG, so that the hydrogen can electrochemically react with air to produce electricity and heat in SOFC. In Table 12, The steam to carbon ratio (S/C) is between 1.25 and 2, and the fuel-to-air ratio varies between 0.04 and 0.06 because of the change of fuel mass flow rates. The difference in fuel mass flow rates is owing to the difference of the heating values of the fuels, which are 77.1 MJ/kg for F1, 52.5 MJ/kg for F2, 74.6 MJ/kg for F3, 75.8 MJ/kg for F4, and 77.7 MJ/kg for F5.

4.2.2. *Effect of fuels on overall turbofan systems*

The alternative fuels are combusted with highly compressed air in the combustion chamber. The existing conditions of the combustion chamber should be 2000 kPa and 1800 K according to the specifications of the Rolls Royce Trent 1000 turbofan engine. In addition, the amount of inlet bypass, and bleeding air is constant throughout the analysis. The fuel mass flow rate varies to ensure adequate combustion based on the heating values of the fuel mixture. Therefore, the fan nozzle conditions are 1099.9 kg/s, 27.1 kPa, 233.2 K, which remain constant. The exhaust conditions vary because of the variation in fuel mass flow rates in the combustion chamber and the fuel cell system, as shown in Table 13. The exhaust temperature of alternative fuels is less than that of kerosene, while the exhaust pressure is more than that of kerosene. This yields more exhaust speed by about 6%.

Using different alternative fuel mixtures affects the thrust force of the hot nozzle. However, the thrust force of the fan nozzle does not change because of the constant air mass flow rate and compressor conditions. As shown in Fig. 5, the hot thrust force reaches a maximum value of 91.1 kN for F2, and a minimum value of 83.4 for F1, the thrust force using kerosene is 83.7 kN. The fan thrust force is about 69 kN. By dividing the fuel mass flow rate by the total thrust force, the TSFC varies from 88.9 to 130.6 kg/(h.kN) for alternative fuels, which are less than that of kerosene of 139.9 kg/(h.kN).

Table 8
Thermodynamic results of the base-turbofan system.

State #	$\dot{m}$ [kg/s]	T [K]	P [kPa]	h [kJ/kg]	s [kJ/kg.K]	ex_{ph} [kJ/kg]	ex_{ch} [kJ/kg]	$\dot{E}x$[kW]
2	1210.0	253.9	40.7	−44.80	0.2505	−74.61	4.48	41300.3
3	1210.0	279.8	57.0	−18.73	0.2514	−48.81	4.48	72589.1
03A	110.1	279.8	57.0	−18.73	0.2514	−48.81	4.48	6605.6
03B	1099.9	279.8	57.0	−18.73	0.2514	−48.81	4.48	65983.5
4	110.1	484.7	340.7	189.99	0.2954	146.79	4.48	16655.7
5	110.1	818.8	2037.6	549.13	0.3401	492.59	4.48	54732.2
05A	107.9	818.8	2037.6	549.13	0.3401	492.59	4.48	53637.5
05B	2.2	818.8	2037.6	549.13	0.3401	492.59	4.48	1094.6
6	113.9	1800.0	2000.0	−548.87	1.3662	1511.33	61.70	179129.3
7	113.9	1515.5	800.0	−940.97	1.3953	1110.57	61.70	133492.6
8	113.9	1350.6	440.0	−1162.92	1.4137	883.14	61.70	107593.6
9	113.9	1127.5	176.0	−1455.28	1.4428	582.08	61.70	73310.8
10	113.9	1127.5	171.0	−1455.28	1.4512	579.59	61.70	73027.2
11	113.9	1127.5	83.6	−1455.28	1.6585	517.76	61.70	65986.5
12	1099.9	233.2	27.1	−18.73	0.4657	−112.69	4.48	6906.3
F1	6.0	293.2	200.0	−2124.03	−7.5357	0.25	47772.49	285107.7

Table 9
Thermodynamic results of components in the base-turbofan engine.

Components	$\dot{Q}$[kW]	$\dot{W}$[kW]	$\dot{E}x_{des}$[kW]	π	η [%]	ψ [%]
FAN	0	31547.2	336.3	1.400	99	98.9
HPC	0	39545.6	1469.1	5.980	90	96.3
HPT	0	44650.2	986.5	0.400	90	97.8
IPC	0	22981.5	1444.1	5.980	90	93.7
IPT	0	25274.8	624.3	0.550	90	97.6
LPT	0	33293.4	989.4	0.400	90	97.1
EN	0	0	7040.7	0.489	87	90.4
FN	0	0	70264.7	0.475	87	41.0
TE	0	0	283.6	0.972	98	99.6
CC	109082.6	0	250639.3	0.982	42.5	41.7

Table 10
Results of the SOFC using F1 (75% methane and 25% hydrogen).

Parameters	Values	Units
VOC	262.35	VA
Number of stacks	36	—
V_{cell}	0.833	V
V_{loss}	0.124	V
$\dot{W}_{SOFC,AC}$	944.4	kW
$\dot{W}_{SOFC,loss}$	141.0	kW
$\dot{Q}_{SOFC,add}$	2928.0	kW
$\eta_{SOFC,e}$	87.0	%
$\eta_{SOFC,th}$	32.3	%
$\psi_{SOFC,th}$	43.9	%

Table 11
Performance of the SR, WGS, and SOFC with respect to fuels.

Parameter	F1	F2	F3	F4	F5
$\dot{Q}_{SR}$ [kW]	1789.0	1084.2	1144.5	1047.1	1260.9
η_{SR} [%]	78.2	47.4	50.0	45.8	55.1
ψ_{SR} [%]	79.5	50.6	50.4	48.7	60.4
$\dot{Q}_{WGS}$ [kW]	111.8	433.8	258.6	353.6	209.2
η_{WGS} [%]	64.8	89.7	86.7	74.3	57.5
ψ_{WGS} [%]	65.1	90.7	89.9	88.5	61.8
$\dot{Q}_{SOFC,add}$ [kW]	2928.0	3102.8	3958.5	3646.4	3360.6
$\eta_{SOFC,th}$ [%]	32.3	30.4	23.9	25.9	28.1
$\psi_{SOFC,th}$ [%]	43.9	41.4	32.5	35.3	38.3

Table 12
Mass flow rates using alternative fuels.

Parameter	Kerosene	F1	F2	F3	F4	F5
$\dot{m}_{F1}$ [kg/s]	5.968	3.90	5.80	4.00	4.00	3.90
F/A [kg_f/kg_a]	0.055	0.040	0.060	0.041	0.041	0.040
$\dot{m}_{F2}$ [kg/s]	—	0.1	0.16	0.15	0.15	0.12
$\dot{m}_{W1}$ [kg/s]	—	0.2	0.2	0.2	0.2	0.2
S/C [kg_w/kg_f]	—	2	1.25	1.33	1.33	1.67

Table 13
Exit conditions of the hot nozzle using different fuels.

Parameters	Kerosene	F1	F2	F3	F4	F5
Exhaust mass flow rate, $\dot{m}_{11}$ [kg/s]	113.9	112.1	114.1	112.3	112.3	112.1
Exhaust Pressure, P_{11} [kPa]	1127.5	1007.9	1036.4	1040.5	1026.1	1033.3
Exhaust Temperature, T_{11} [K]	83.6	101.6	113.7	118.0	110.0	113.7
Exhaust speed, U_{11} [m/s]	607.8	643.2	657.5	621.2	648.8	657.5

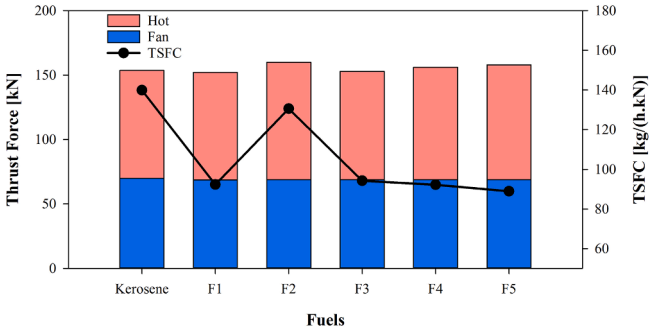

Fig. 5. Thrust force and the TSFC of the base- and SOFC -turbofans with respect to fuels.

The net power of GT and thrust energy is displayed in Fig. 6. Using kerosene can achieve a maximum net power of 9144 kW because of the high mass flow rate of 6 kg/s for alternative fuels, the F5 achieves a minimum net power of 5768 kW, and the F1 can achieve a maximum power of 8730 kW. The thrust energy can be obtained to be 38.2 MW for

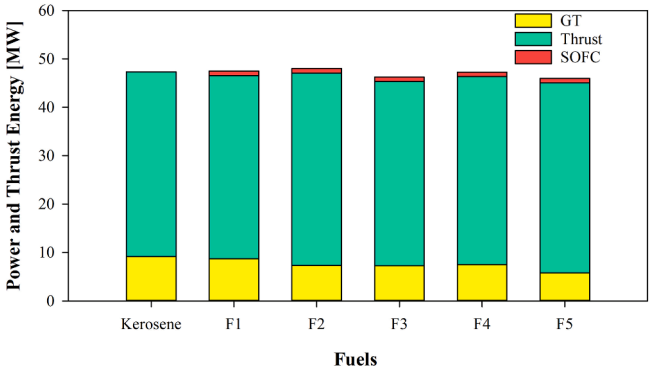

Fig. 6. Net power of the GT and thrust energy of the base- and SOFC-turbofans.

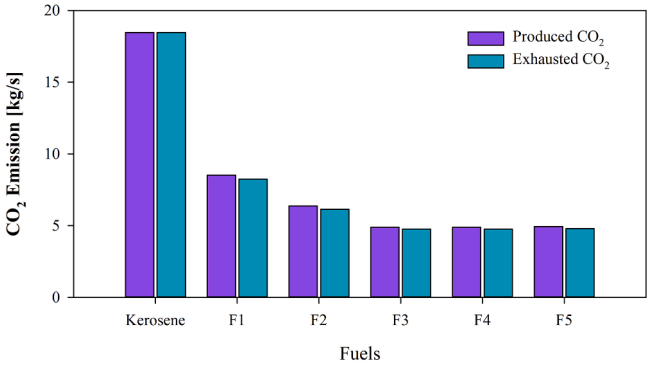

Fig. 8. CO_2 emission with respect to fuels.

kerosene, while the maximum and minimum thrust energy can be reached 39.8 MW for F3 and 37.8 MW for F1, respectively. The net power of SOFC is constant and equivalent to 944.4 kW. Therefore, the total power of 48 MW can be achieved using F2, which is an increase of 1.5% compared to that of kerosene.

The overall thermal and exergetic efficiencies of the turbofan engines are displayed in Fig. 7. Fuel of F3 achieves the highest thermal and exergetic efficiencies of 48.1% and 54.4%, respectively. Using kerosene fuel reduced the thermal efficiency to 43.4%, but the exergetic efficiency is about 52% and is the third-highest value.

The environmental impact is studied by estimated the CO_2 emissions and presented in Fig. 8. The kerosene fuel produces CO_2 of 18.5 kg/s and emits the amount to the atmosphere. This amount can be decreased by 54% using F1, 65% using F2, and about 73% using F3, F4, and F5, reaching 4.9 kg/s without using the SOFC system. SOFC system reduces the CO_2 emission by about 3.5% for all alternative fuel mixtures. The minimum production and exhaustion of CO_2 can be achieved by using F3 and F4, reaching 4.75 kg/s. These fuels are ethanol- and dimethyl ether-based fuels since they have similar chemical formulas and molecular weight.

4.2.3. *Effect of fuel mass flow rate*

The effect of fuel F1 mass flow rate on hybrid turbofan engine is shown in Fig. 9. The compression and turbine pressure ratio, maximum TIT, and inlet air mass flow rate are remaining constant. The fuel mass flow rate varies from 3 to 10 kg/s. The combustion heat rapidly increases from 58 MW to 176 MW at 5.6 kg/s, then gradually decreases to 100 MW at 10 kg/s. The net power and thrust force gradually increased from about 6 to 40 MW and 150 to 173 kN, respectively. This results in the thermal efficiency decreasing from 78 to 30% then increases to 88%, and the exergetic efficiency has the same trend but 5% higher.

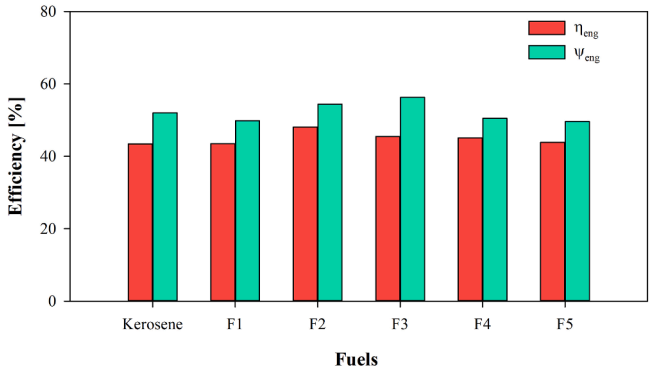

Fig. 7. Overall thermal and exergetic efficiencies of the base- and SOFC-turbofans.

4.2.4. *Effect of combustion pressure*

The effect of combustion pressure on the hybrid turbofan engine is displayed in Fig. 10 using fuel F1, while the TIT, inlet air, and fuel mass flow rate are 1800 K, 1210, and 6 kg/s, which remain constant. Increasing the combustion pressure from 1900 to 2500 kPa does not affect the combustion heat, which is about 104.2 MW. Consequently, the net power remains almost constant, about 8.7 MW, but the thrust force increases from 152.5 to 156.5 kN. Therefore, the thermal and exergetic efficiencies slightly increased from 43.6 to 44.2% and 40.6 to 41.5%, respectively.

5. Conclusions

This paper conducted thermodynamic analyses to investigate the performance of a proposed hybrid turbofan consisting of the turbofan of the Rolls and Royce Trend 1000 and the SOFC system. The SOFC system contains the steam reforming and water gas shift. Kerosene is used as the traditional, fossil-based fuel, whereas hydrogen, methane, methanol, ethanol, and dimethyl ether are selected as the alternative fuels to replace kerosene. The conclusions from this study are listed below:

- The base turbofan can produce a net power of 9144 kW and a thrust energy of 38 MW, with a 43.4% thermal efficiency and a 52% exergetic efficiency at cruising conditions.
- The SOFC can deliver a net power of 944 kW with an electric efficiency of 87.0%, thermal efficiency of 32.3%, and exergetic efficiency of 43.9% using F1 (75% methane and 25% hydrogen) fuel, which achieves the maximum performance in the SOFC system.
- The exhaust speed at the hot nozzle can reach a maximum value of 657.5 m/s using F2 (75% methanol and 25% hydrogen) and F5 (15% methane, 40% hydrogen, 15% methanol, 15% ethanol, and 15% DME), but F2 can provide the highest thrust force of 160 kN with a high TSFC of 130 kg/(h.kN).
- The maximum total power of 48 MW can be obtained using F2, including 7.3 MW of net power of the gas turbine, 39.8 MW of thrust energy, and 0.94 MW of the SOFC system.
- The overall thermal and exergetic efficiencies of the hybrid turbofan are 48.1% and 54.4%, respectively, using F2.
- Alternative fuel mixture can reduce CO_2 emission by 54% for F1, 65% using F2 and 73% for F3 (60% ethanol and 40% hydrogen), F4 (60% DME and 40% hydrogen) and F5.
- Increasing the fuel mass flow rate of F1 to more than 5 kg/s increases the performance of the hybrid turbofan.
- Increasing the combustion pressure has only a slight effect on net power and thrust force and no significant effect on the thermal and exergetic efficiencies.
- The fuel F3, consisting of 60% ethanol and 40% hydrogen can achieve thermal and exergetic efficiencies of 46% and 56%, respectively.

It is recommended that exergoeconomic and exergoenvironmental

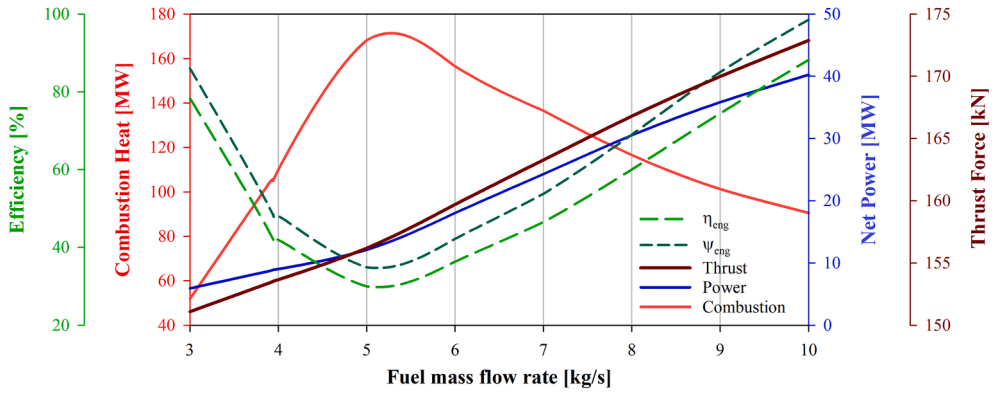

Fig. 9. Effect of fuel mass flow rate using F1 (75% methane and 25% hydrogen).

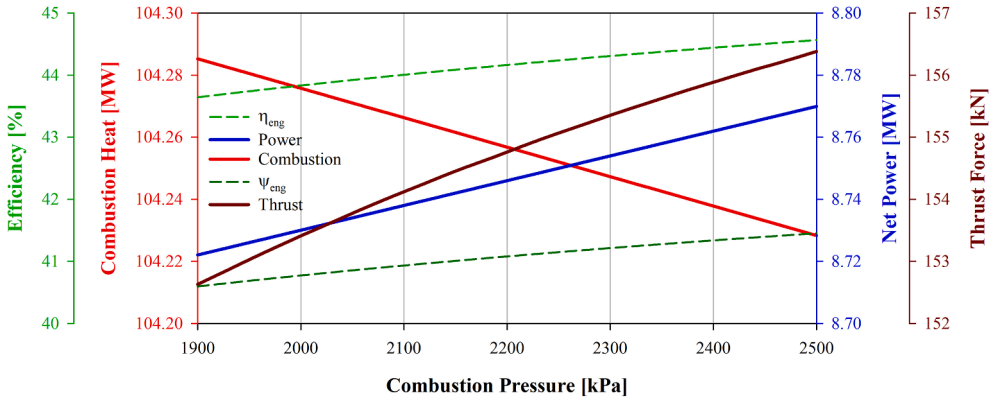

Fig. 10. Effect of combustion pressure using F1 (75% methane and 25% hydrogen).

analyses be performed on the aviation engines to provide a comprehensive understanding of the proposed system with respect to the traditional engines.

CRediT authorship contribution statement

Shaimaa Seyam: Conceptualization, Data curation, Formal analysis, Investigation, Methodology, Software, Supervision, Validation, Visualization, Writing - original draft, Writing - review & editing. **Ibrahim Dincer:** Supervision, Conceptualization, Funding acquisition, Writing - review & editing, Project administration, Resources. **Martin Agelin-Chaab:** Co-supervision, Conceptualization, Funding acquisition, Writing - review & editing, Project administration, Resources.

Declaration of Competing Interest

The authors declare that they have no known competing financial interests or personal relationships that could have appeared to influence the work reported in this paper.

Acknowledgment

The financial support provided by the Natural Sciences and Engineering Research Council of Canada (NSERC) and Transport Canada through their Clean Transportation System-Research & Development Program is gratefully acknowledged.

References

[1] Natural Resources Canada. Transportation Sector – Energy Use Analysis | Natural Resources Canada. Nat Resour Canada 2019. https://oee.nrcan.gc.ca/corporate/statistics/neud/dpa/showTable.cfm?type=AN&sector=tran&juris=00&rn=1&page=0 (accessed January 14, 2021).
[2] Natural Resources Canada. Energy Fact Book 2020-2021. 2020.
[3] Government of Canada. Canada's Action Plan to reduce greenhouse gas emissions from aviation. 2019.
[4] Kousoulidou M, Lonza L. Biofuels in aviation: Fuel demand and CO2 emissions evolution in Europe toward 2030. Transp Res Part D Transp Environ 2016;46:166–81. https://doi.org/10.1016/j.trd.2016.03.018.
[5] Badami M, Nuccio P, Pastrone D, Signoretto A. Performance of a small-scale turbojet engine fed with traditional and alternative fuels. Energy Convers Manag 2014;82:219–28. https://doi.org/10.1016/j.enconman.2014.03.026.
[6] Aydin E, Turan O, Kose R. Exergy analysis of a target drone engine: An experimental study for TRS18. Int J Exergy 2018;27:206–30. https://doi.org/10.1504/IJEX.2018.094595.
[7] Yazar I, Söhret Y, Karakoç TH. ANFIS-based comparative exhaust gases emissions prediction model of a military aircraft engine. Int J Global Warming 2017;12(1):116–28. https://doi.org/10.1504/IJGW.2017.084018.
[8] Hashemi SR, Baghbadorani AB, Esmaeeli R, Mahajan A, Farhad A. Machine learning-based model for lithium-ion batteries in BMS of electric/hybrid electric aircraft. Int J Energy Res 2021;45(4):5747–65. https://doi.org/10.1002/er.6197.
[9] Petrescu RVV, Machín A, Fontánez K, Arango JC, Márquez FM, Petrescu FIT. Hydrogen for aircraft power and propulsion. Int J Hydrogen Energy 2020;45:20740–64. https://doi.org/10.1016/j.ijhydene.2020.05.253.
[10] Mze Ahmed A, Mancarella S, Desgroux P, Gasnot L, Pauwels JF, El Bakali A. Experimental and numerical study on rich methane/hydrogen/air laminar premixed flames at atmospheric pressure: effect of hydrogen addition to fuel on soot gaseous precursors. Int J Hydrogen Energy 2016;41:6929–42. https://doi.org/10.1016/j.ijhydene.2015.11.148.
[11] Valera-Medina A, Morris S, Runyon J, Pugh DG, Marsh R, Beasley P, et al. Ammonia, methane and hydrogen for gas turbines. Energy Procedia 2015;75:118–23. https://doi.org/10.1016/j.egypro.2015.07.205.
[12] Jia T, Gong S, Pan L, Deng C, Zou JJ, Zhang X. Impact of deep hydrogenation on jet fuel oxidation and deposition. Fuel 2020;264:116843. https://doi.org/10.1016/j.fuel.2019.116843.
[13] Cai T, Zhao D. Effects of fuel composition and wall thermal conductivity on thermal and NOx emission performances of an ammonia/hydrogen-oxygen micro-power system. Fuel Process Technol 2020;209:106527. https://doi.org/10.1016/j.fuproc.2020.106527.
[14] Luo F, Song W, Chen W, Long Y. Investigation of kerosene supersonic combustion performance with hydrogen addition and fuel additive at low Mach inflow conditions. Fuel 2021;285:119139. https://doi.org/10.1016/j.fuel.2020.119139.

[15] Bicer Y, Dincer I. Life cycle evaluation of hydrogen and other potential fuels for aircrafts. Int J Hydrogen Energy 2017;42:10722–38. https://doi.org/10.1016/j.ijhydene.2016.12.119.
[16] Ji Z, Qin J, Cheng K, Liu H, Zhang S, Dong P. Performance evaluation of a turbojet engine integrated with interstage turbine burner and solid oxide fuel cell. Energy 2019;168:702–11. https://doi.org/10.1016/j.energy.2018.11.088.
[17] Waters DF, Cadou CP. Engine-integrated solid oxide fuel cells for efficient electrical power generation on aircraft. J Power Sources 2015;284:588–605. https://doi.org/10.1016/j.jpowsour.2015.02.108.
[18] Ji Z, Qin J, Cheng K, Dang C, Zhang S, Dong P. Thermodynamic performance evaluation of a turbine-less jet engine integrated with solid oxide fuel cells for unmanned aerial vehicles. Appl Therm Eng 2019;160:114093. https://doi.org/10.1016/j.applthermaleng.2019.114093.
[19] Bakalis DP, Stamatis AG. Optimization methodology of turbomachines for hybrid SOFC-GT applications. Energy 2014;70:86–94. https://doi.org/10.1016/j.energy.2014.03.093.
[20] Ji Z, Rokni MM, Qin J, Zhang S, Dong P. Energy and configuration management strategy for battery/fuel cell/jet engine hybrid propulsion and power systems on aircraft. Energy Convers Manag 2020;225:113393. https://doi.org/10.1016/j.enconman.2020.113393.
[21] Verstraete D. Long range transport aircraft using hydrogen fuel. Int J Hydrogen Energy 2013;38:14824–31. https://doi.org/10.1016/j.ijhydene.2013.09.021.
[22] Canada's climate plan - Canada.ca n.d. https://www.canada.ca/en/services/environment/weather/climatechange/climate-plan.html (accessed November 30, 2019).
[23] EASA. Type-certificate data sheet for Trent 1000 series engines. 2019.
[24] Atkinson A, Marquis AJ. Handbook of Fuel Cells. 2010. doi:10.1002/9780470974001.f500032.
[25] Minutillo M, Perna A, Jannelli E. SOFC and MCFC system level modeling for hybrid plants performance prediction. Int J Hydrogen Energy 2014;39:21688–99. https://doi.org/10.1016/j.ijhydene.2014.09.082.
[26] Bessette NF, Wepfer WJ. A mathematical model of a tubular solid oxide fuel cell. J Energy Resour Technol Trans ASME 1995;117:43–9. https://doi.org/10.1115/1.2835319.
[27] Milewski J, Swirski K, Santarelli M, Leone P. Advanced mehtods of solid fuel cell modeling 2011.
[28] Badwal SPS, Giddey S, Kulkarni A, Goel J, Basu S. Direct ethanol fuel cells for transport and stationary applications - A comprehensive review. Appl Energy 2015;145:80–103. https://doi.org/10.1016/j.apenergy.2015.02.002.
[29] Semelsberger TA, Borup RL, Greene HL. Dimethyl ether (DME) as an alternative fuel. J Power Sources 2006;156:497–511. https://doi.org/10.1016/j.jpowsour.2005.05.082.
[30] Matzen M, Demirel Y. Methanol and dimethyl ether from renewable hydrogen and carbon dioxide: Alternative fuels production and life-cycle assessment. J Clean Prod 2016;139:1068–77. https://doi.org/10.1016/j.jclepro.2016.08.163.
[31] Yuan W, Frey HC, Wei T, Rastogi N, VanderGriend S, Miller D, et al. Comparison of real-world vehicle fuel use and tailpipe emissions for gasoline-ethanol fuel blends. Fuel 2019;249:352–64. https://doi.org/10.1016/j.fuel.2019.03.115.
[32] Li Q, Wu G, Johnston CM, Zelenay P. Direct Dimethyl Ether Fuel Cell with Much Improved Performance. Electrocatalysis 2014;5:310–7. https://doi.org/10.1007/s12678-014-0196-z.
[33] Pereira LG, Cavalett O, Bonomi A, Zhang Y, Warner E, Chum HL. Comparison of biofuel life-cycle GHG emissions assessment tools: The case studies of ethanol produced from sugarcane, corn, and wheat. Renew Sustain Energy Rev 2019;110:1–12. https://doi.org/10.1016/j.rser.2019.04.043.
[34] McCarty RD, Hord J, Roder HM. Selected Properties of Hydrogen (Engineering Design Data). U.S. Department of Commerce/National Bureau of Standards; 1981.
[35] Cengel YA, Boles MA. Thermodynamics: A Engineering Approach. Eighth. McGraw-Hill Education, USA; 2015. doi: 10.1109/MILCOM.2005.1605829.
[36] Verhelst S, Turner JW, Sileghem L, Vancoillie J. Methanol as a fuel for internal combustion engines. Prog Energy Combust Sci 2019;70:43–88. https://doi.org/10.1016/j.pecs.2018.10.001.
[37] Shehata MS, Elkotb MM, Salem H. Combustion characteristics for turbulent prevaporized premixed flame using commercial light diesel and kerosene fuels. J Combust 2014;2014. https://doi.org/10.1155/2014/363465.
[38] Physical Property Data: Reference Manual, Version 10. Aspen Technology Inc; 1999.
[39] Sandler SI. Using Aspen Plus ® in Thermodynamics Instruction: A Step-by-Step Guide; AICHE - Wiley; 2015.
[40] Peng DY, Robinson DB. A New Two-Constant Equation of State. Ind Eng Chem Fundam 1976;15:59–64. https://doi.org/10.1021/i160057a011.
[41] Aygun H, Cilgin ME, Ekmekci I, Turan O. Energy and performance optimization of an adaptive cycle engine for next generation combat aircraft. Energy 2020;209:118261. https://doi.org/10.1016/j.energy.2020.118261.
[42] Zhang W, Croiset E, Douglas PL, Fowler MW, Entchev E. Simulation of a tubular solid oxide fuel cell stack using AspenPlus™ unit operation models. Energy Convers Manag 2005;46:181–96. https://doi.org/10.1016/j.enconman.2004.03.002.
[43] AspenTech. Aspen Plus 11.1 User Guide. Engineering 2001:2–18. doi:10.3991/ijoe.v11i9.5065.